

(DGMs) which can serve as \mathbb{Z}_2 candidates, by calculating the invariant for materials where the valence and conduction band manifolds are separated by a direct gap (DG), but where the indirect gap (IG) is negative.

II. METHODS

All the density-functional theory (DFT) calculations performed in this work use the Quantum ESPRESSO (QE)^{41,42} distribution. We perform fully relativistic calculations with SOC, using the Perdew, Burke and Ernzerhof (PBE) pseudopotentials⁴³ from the ONCVSP (v0.4) set⁴⁴ contained in the PseudoDojo library⁴⁵. For every calculations we use a kinetic cutoff, high enough to ensure that the uncertainty on the energy eigenvalues is lower than 5 meV. In order to properly account for low-gap and metallic systems, a Fermi-Dirac smearing of 5 meV is used. For the initial self consistent calculations we use a \mathbf{k} -point mesh of density 0.2 \AA^{-1} , which is refined to 0.1 \AA^{-1} for QSHI candidates. All the calculations have been performed assuming a non-magnetic ground state, magnetism has been later checked for the selected candidates following the same approach used in Ref.18.

The topological invariant are computed either from an analysis of the band structures at the TRIM points or using the Z2Pack package⁴⁶, for which we set the maximum number of k-points per line to 200, and the lowest acceptable distance between lines to 10^{-7} . The threshold on the hybrid Wannier charge centers (HWCC)⁴⁷ position variation per step on a line (pos_tol) is set to 0.01, the threshold on the relative movement of the HWCCs position between neighboring (move_tol) to 0.3 and the threshold for the distance between the middle of the largest gap in a line and the position of the neighboring HWCC (gap_tol) to 0.3.

For the new QSHI found, we also perform a hybrid functional calculation, using HSE06⁴⁸. We find that in order to obtain a properly converged Wannierization of the system, a very dense $32 \times 16 \times 1$ k-point mesh with a $4 \times 2 \times 1$ q-point mesh has to be used. The Wannierized wavefunctions are then used to compute the topological invariant and edge states, in order to confirm whether the system remains a topological insulator.

A. Screening procedure

The original set of material of which we explore the properties is derived from the ICSD^{49,50}, COD⁵¹ and MPDS⁵² databases, by identifying 2D exfoliable materials, starting from experimentally known bulk structures using vdW DF2-C09 DFT calculations¹⁸. First we exclude all materials containing lanthanides, due to the inaccuracy of plain DFT pertaining calculations with these atoms caused by the presence of strongly correlated electrons⁴⁰. For the remaining 603 materials, compared to the 1306 structures studied in Ref 12 by Marrazzo

et al, we follow two strategies for the identification of QSHIs in order to minimize the usage of computational resources. For the ones with inversion symmetry we use the formula given by Fu and Kane²⁵

$$(-1)^\nu = \prod_i \delta_i, \quad \delta_i = \prod_{m=1}^N \xi_{2m}(\Gamma_i) \quad (1)$$

where ν is the \mathbb{Z}_2 topological invariant, ξ_{2m} is the eigenvalue of the parity operator calculated for a couple of TR-paired bands and Γ_i are the TRIM points, of which there are 4 for a 2D material, defined as

$$\Gamma_i = -\Gamma_i + \mathbf{G} \quad (2)$$

with \mathbf{G} being any reciprocal lattice vector. For a 2D material, 4 TRIM points can be found at the coordinates (0,0), (0,0.5), (0.5,0) and (0.5,0.5) expressed in units of the reciprocal lattice vector. Given the formula in eq.(1), the most computationally efficient route for materials that have inversion symmetry is to calculate first the band structure at the TRIM points to determine the topological invariants. Materials with $\nu = 0$ are discarded, while for those with $\nu = 1$ we proceed with a band structure calculation along the high-symmetry lines. The result can either be a material with finite DG on the entire \mathbf{k} -point path, or with a zero DG. The latter is discarded as a metal/semimetal without an isolated valence band manifold, while the former can either be a QSHI if the IG, defined as the difference between the minimum of the conduction band and the maximum of the valence band, is positive, or a DGM if the IG is negative. The values of the DGs and IGs are further corroborated by analyzing the band structure computed on a dense uniform k-point grid with a spacing of 0.015 \AA^{-1} . We discard materials that are DGM with an IG lower than -0.15 eV, as attempting to drive such a material to a topological phase would be hardly feasible. The same band structure on the dense uniform grid is also used to derive the density of states (DOS) for the materials studied.

If inversion symmetry is not present, we follow a different route, by determining the DG and IG first through a band structure calculation and discarding the metals and semimetals without a finite DG. We then use the Z2Pack package, which tracks the positions of one-dimensional HWCCs across half of the BZ, in order to compute the topological invariant⁵³. The package acts as an automation tool, which interfaces a DFT code (QE in our case) with Wannier90⁵⁴ in order to calculate the HWCC positions on a progressively denser grid of \mathbf{k} -points. If one of the convergence criteria of Z2Pack, with the parameters mentioned before, is not satisfied, then the material is discarded. If the results of the calculation is a non trivial topological invariant, the material is then classified as a QSHI or DGM following the same criteria mentioned for the inversion-symmetric cases, where the direct and indirect gaps are then checked again from the band structures on a dense k-point grid used also for the DOS.

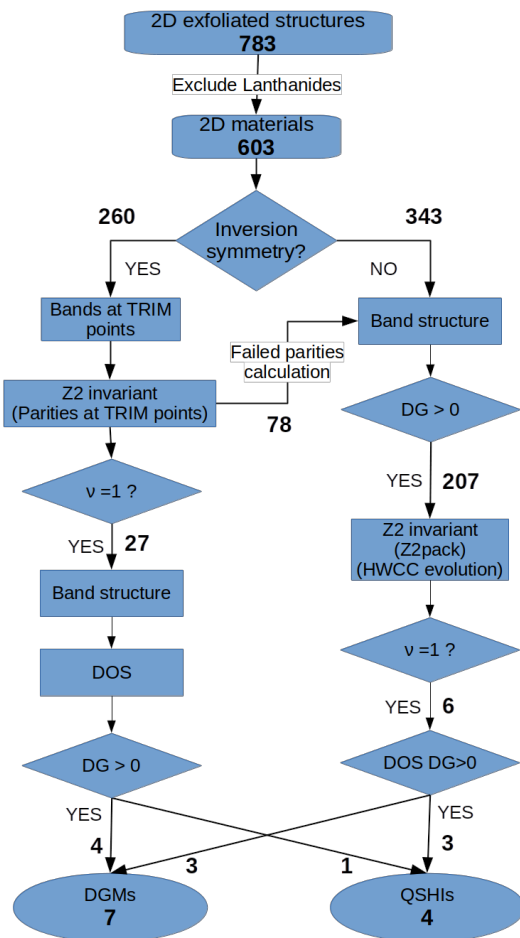


FIG. 1: Workflow adopted for the high-throughput screening of the QSHIs. Starting from 783 structures presented in Ref 39 we proceed to a study of the \mathbb{Z}_2 topological invariant following two branches, depending on the presence of inversion symmetry in the material. The steps in both branches are organized as to limit the usage of resources, by performing the lowest cost screenings first in each branch.

Finally, for the selected candidates we assess the dynamical stability by computing the full phonon dispersion by means of density-functional perturbation theory⁵⁵ and we check the non-magnetic ground state assumption comparing the energy of the non-magnetic ground state with different possible ferromagnetic, antiferromagnetic and ferrimagnetic configurations following the same procedure adopted in Ref. 18. A flowchart describing the entire high-throughput calculation is shown in Fig. 1. The entire process has been automated using AiiDA^{56,57}, a workflow managing infrastructure, which enable us to keep track of the provenance at every computational step. The data produced in this work, including both the results and the entire provenance tree, has been made available on the Materials Cloud as Ref. 58.

III. RESULTS AND DISCUSSIONS

We start our screening from a set of 783 2D exfoliable structures taken from Ref 39, which are reduced to 603 after removing materials containing lanthanides. The set is further divided in two groups of 260/342 structures with/without inversion symmetry. For the inversion symmetric materials, we compute the eigenvalues of the parity operator ξ_{2m} , the calculation of which can sometimes fail due to limitations in the code to handle non-symmorphic space groups, or due to the accuracy threshold imposed for the calculation of the trace of the representation for each group of bands. 78 out of these 260 TRIM point calculation failed and were hence recalculated using Z2pack. Of the 182 successful calculations, 27 resulted in a non trivial topological invariant $\nu = 1$. We then performed a band structure calculations along the high-symmetry path⁵⁹, from which we excluded 22 metallic materials and identified 1 QSHI (HfBr) and 4 direct gap metals (DGMs).

On the 343+78 remaining structures (the non-inversion symmetric ones and those with failed parity calculations), the band structure calculations show that 207 materials have a DG greater than 0; for them we proceed with Z2Pack calculations that identify, 3 QSHIs (ZrTe₅, HgNS, HfTe₅) and 3 DGMs. The summary of the data for every material is reported in Table I, while a more detailed report is given in the supplementary materials⁶⁰, together with the crystal structure and band structure of the material identified and a plot of the HWCC for every Z2Pack calculation.

A summary for all the materials analyzed in the present work, together with those of the previous screening by Marrazzo et al.¹² (in absence of strain), is shown in Fig. 2, where the QSHIs are highlighted. In the figure, all materials with a negative IG have been put on the $y = 0$ axis in order to emphasize QSHIs and DGMs, especially with regard to the magnitude of the DG and IG, as these two parameters can be used to determine the range of temperatures at which a device could operate⁶¹.

The interest in DGMs with a non trivial ν is twofold. First it is possible that, given the limitations of DFT-PBE calculations, the band gap of the material is being underestimated and, using more appropriate methods (such as many-body perturbation theory in the GW approximation⁶²), a material that was computed to be a DGM with DFT-PBE could actually result to be a QSHI. It is worth highlighting that the opposite could also be possible, where a material that is estimated to be a QSHI within DFT-PBE could end up being a trivial insulator in a GW calculation (as discussed for the case of TiNi in Ref.¹²). Second, a DGM could be driven into a \mathbb{Z}_2 topological state through an external perturbation that could open a gap in the material without driving a band inversion^{29,30}. To this end, it is important to look at both the IG and DG of the material. The former is related to how strong a perturbation needs to be in order to drive the material in a semiconducting state, while the latter

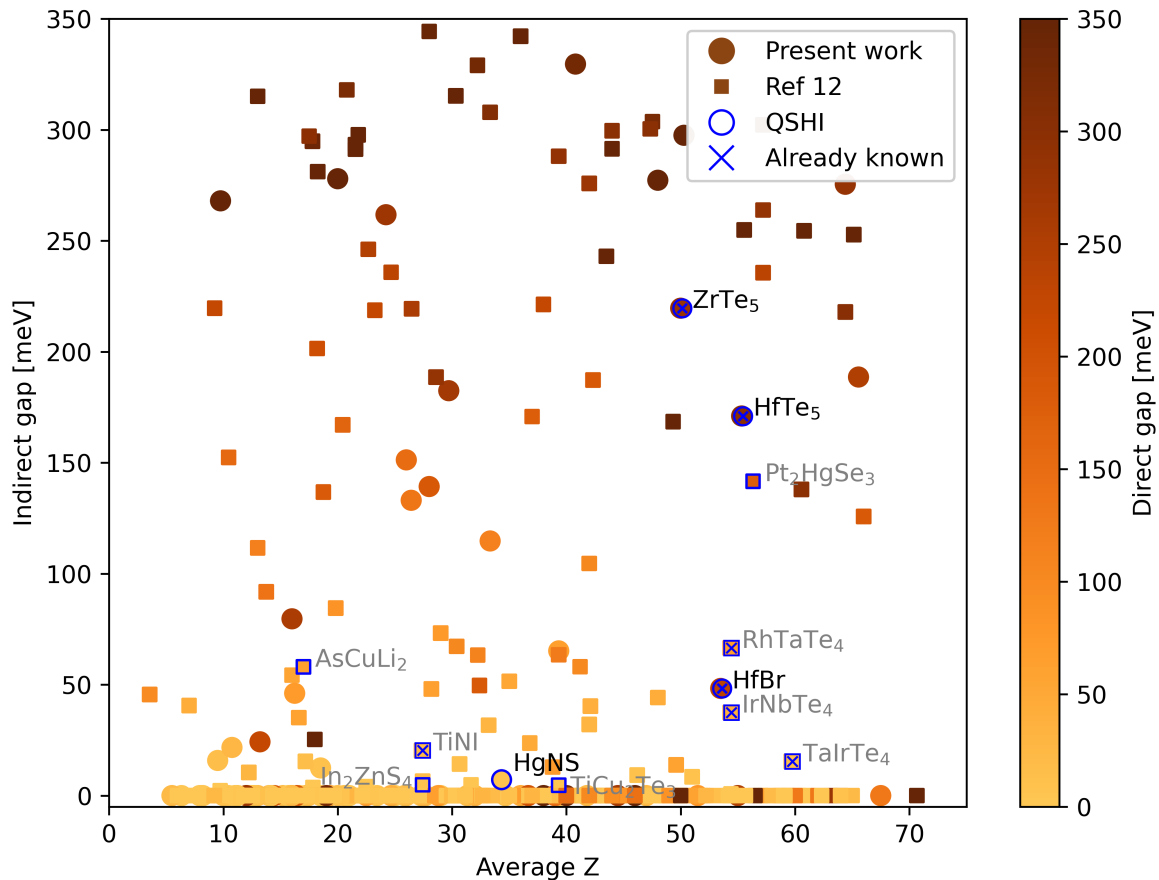


FIG. 2: Plot of the direct (color scale) and indirect (y-axis) band gaps in the presence of SOC for all the material screened in the current work (circles) and in the previous work of Marrazzo et al.¹² (squares). Materials with negative IGs have been given a zero value. The DG for each material is given using the color scale on the right. QSHIs identified by the present screening effort and that of Ref 12 are highlighted using a blue contour to the circle/squares. Materials already known in the literature are also highlighted with a cross mark.

gives us an idea of how likely it is that a gap could be opened, without causing band inversion, or driving the material into a metallic state. Indeed, the higher the DG of a material, the more difficult it will be to close it. For this reason, DGMs with small negative IG and large DG are prime candidates for further studies; a visual summary of the direct and indirect gap of the DGMs is shown in Fig. 3. Among the various possible perturbations that could open the gap, the most interesting ones, from the standpoint of applications in a device, would be gating/electric fields²⁷, the interaction with a substrate⁶³ and/or the application of strain⁶⁴.

For all the materials found, we searched the current literature to determine which QSHIs were already known, and which one are novel to this study. We find that among the 4 QSHIs identified, 3 were already known, namely the two tellurides of hafnium/zirconium, and hafnium bromide. HfBr^{65,66} was already known both for being an easily exfoliable material and for its topological properties in its 2D and 3D forms. This material has a

DG of 233 meV and an IG of 48 meV making it a good candidate for experiments and possible device realization. It should also be noted that this material belongs to a broader class of transition-metal halides MX (M=Zr, Hf X=Cl, Br) which has already been predicted to host topological properties. Furthermore, several class of similar honeycomb materials have also been predicted to host topological states such as transition metal carbides MC (M=Ti, Zr, Hf)⁶⁷ and transition metal compounds MM' (M=Ti, Zr, Hf) (M'=Bi, Sb)⁶⁸.

HfTe₅ (ZrTe₅)⁶⁹ are two pentatellurides both of which have large DGs of 300(281) meV and IGs of 171(220) meV making them both very good candidates for QSHIs applications at room temperature. Interestingly, as shown by Weng et al.⁶⁹, the presence of a band inversion in these materials comes mainly from the non-symmorphic features of their space group which, together with the presence of 2 non-equivalent Te atom chains, drives the ordering of the bands at Γ . At the same time, the symmetries of the space group give raise to four-fold

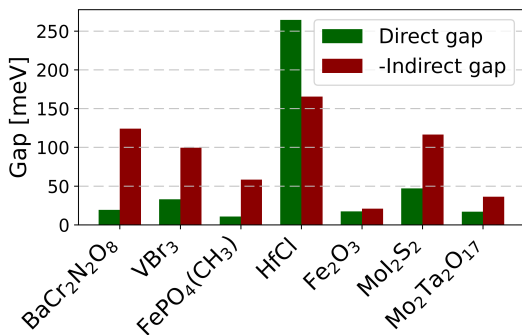


FIG. 3: Plot of the direct and indirect band gaps of the DGMs identified. The criteria used are that the material has to exhibit $DG > 0$ (which allows for the calculation of \mathbb{Z}_2 on an isolated manifold) and a negative IG < 300 meV. These materials would become QSHIs in the presence of perturbations such as strain, substrate interactions or an electric field capable of opening the IG without causing a band inversion.

degenerate bands at the TRIM points, 2 with even and 2 with odd parity, such that the presence of SOC will only open a gap in a band structure that would otherwise be metallic, but will preserve the product of parity eigenvalues at the TRIM points. These pentatellurides have also been proposed for the realization of the quantum anomalous Hall effect, when the transition metal Hf/Zr is substituted for a rare earth metal which could induce a magnetic ordering in the material, breaking time-reversal symmetry^{69,70}.

HgNS is a new compound which has not been discussed in the literature for its topological properties. Its direct and indirect gaps are both of 7 meV. Such low gap, in between that of silicene (1.4 meV) and germanene (23.8 meV) precludes room temperature applications. Nevertheless, at the gap, situated along the $\Gamma - Y$ direction, the material shows a linear band dispersion akin to that of germanene at K when SOC is taken into account. The similarity between the two systems, opens the possibility for a multitude of studies, such as the effect of an electric field on the gap and band inversion^{27,28} or the possibilities for opto-electronic applications in THz devices⁷¹. Given that HgNS would constitute a new QSHI, we also study it using the hybrid HSE06 functional as described in the methods. We find, as expected, that the effect of the hybrid is that of increasing the gap in the material. We can also observe from the band structure shown in the supplementary material⁶⁰ that the gap opening goes against the band inversion, moving the quasi-linear crossing toward the edge of the zone, but is not strong enough to drive the material to a trivial states. Hence, we find that HgNS is still a QSHI, as corroborated by the HWCCs evolution and edge state calculations shown in the supplementary material⁶⁰, even when a hybrid functional is used, and

the gap increases from 7 meV to 38 meV.

Among the DGMs, the most promising ones are Fe₂O₃ and Mo₂Ta₂O₁₇, with small IGs of -21 and -36 meV respectively. The small negative IGs indicate that it could be feasible to force those from being DGM to a QSHI by acting via strain, electric field or other perturbations. There is also HfCl which, like HfBr, is a transition metal halide and has been studied in Ref 65, in which the material is identified as a semi-metal for both PBE and PBE-SOC calculations, but as QSHI in a HSE06-SOC calculation. This reiterates that DGMs identified by DFT can or could actually be found to be QSHIs if studied with techniques, such as many body perturbation theory, that can correctly estimate the gap, or when exposed to a perturbation.

When considering the QSHIs identified in this work, we obtain a relative abundance of topological insulators of 0.5%, which goes up to 1.4% if the DGMs are included as well. This result is comparable to that of the previous work of Marrazzo et al¹² where an abundance of 1.1% was found for QSHIs. The difference in the values can be explained by two reasons: first, in the work from Marrazzo, strained configurations had also been considered when determining a material topology. Second, when analyzing the space group distributions of the two datasets, shown in Fig. SM1-2, we can observe that the old dataset contained more materials with monoclinic Bravais lattice, in particular with space group 11, which from the analysis seems to be the one with the most QSHIs and DGMs when compared to all other space groups.

IV. CONCLUSIONS

We performed a systematic high-throughput study of 2D exfoliable materials in order identify novel QSHIs. Starting from a set of 783 materials we found 4 QSHIs (1 novel) and 7 DGMs (6 novel) that could be driven into a QSHI state by material engineering, for a relative abundance of 0.5% for QSHIs and 1.4% if DGMs are also included. Of the 4 QSHIs identified, the 3 with the largest gaps had already been explored in the literature. In particular, the two pentatellurides HfTe₅ and ZrTe₅ exhibit both large direct and indirect gaps which makes them promising candidates for room-temperature applications. The remaining material, namely HgNS, represents a newly identified QSHI with linear bands in proximity of its direct gap of 38 meV when computed with an hybrid HSE functional. The main feature of this material is the small gap and band linearity, akin to that of silicene or germanene. For this reason, HgNS could be a promising candidate for future electronic and photonic applications in the low energy regime.

All materials identified in this work are easily exfoliable, with a binding energy lower than 20 meV/Å²¹⁸ and for this reason they are prime candidates for possible experimental realization through exfoliation techniques starting from their experimentally known 3D bulk form.

V. ACKNOWLEDGMENTS

This work was supported by the National Centre for Computational Design and Discovery on Novel Materials (NCCR MARVEL) of the Swiss National Science Foundation. D.G. gratefully acknowledge support from the EU Centre of Excellence, MaX Materials design at the

eXascale (Grant 824143). We acknowledge PRACE for awarding us access to Marconi at Cineca, Italy (project id. 2016163963). A.M. acknowledges financial support from ICSC - Centro Nazionale di Ricerca in High Performance Computing, Big Data and Quantum Computing, funded by European Union - NextGenerationEU

-
- * davide.grassano@epfl.ch
- ¹ J. Wang and S.-C. Zhang, *Nature materials* **16**, 1062 (2017).
 - ² Q. Niu, D. J. Thouless, and Y.-S. Wu, *Physical Review B* **31**, 3372 (1985).
 - ³ L. Fu and C. L. Kane, *Physical Review B* **74**, 195312 (2006).
 - ⁴ A. A. Soluyanov, *Topological aspects of band theory*, Ph.D. thesis, Rutgers University (2012).
 - ⁵ C. L. Kane and E. J. Mele, *Physical Review Letters* **95**, 146802 (2005).
 - ⁶ X. Dai, T. L. Hughes, X.-L. Qi, Z. Fang, and S.-C. Zhang, *Physical Review B* **77**, 125319 (2008).
 - ⁷ C. Timm, *Physical Review B* **86**, 155456 (2012).
 - ⁸ S. Rachel and M. Ezawa, *Physical Review B* **89**, 195303 (2014).
 - ⁹ D. A. Abanin, P. A. Lee, and L. S. Levitov, *Solid state communications* **143**, 77 (2007).
 - ¹⁰ G. J. Ferreira and D. Loss, *Physical Review Letters* **111**, 106802 (2013).
 - ¹¹ X. Li, Z. Zhang, Y. Yao, and H. Zhang, *2D Materials* **5**, 045023 (2018).
 - ¹² A. Marrazzo, M. Gibertini, D. Campi, N. Mounet, and N. Marzari, *Nano Letters* **19**, 8431 (2019).
 - ¹³ T. Olsen, E. Andersen, T. Okugawa, D. Torelli, T. Deilmann, and K. S. Thygesen, *Physical Review Materials* **3**, 024005 (2019).
 - ¹⁴ M. Vergniory, L. Elcoro, C. Felser, N. Regnault, B. A. Bernevig, and Z. Wang, *Nature* **566**, 480 (2019).
 - ¹⁵ F. Tang, H. C. Po, A. Vishwanath, and X. Wan, *Nature* **566**, 486 (2019).
 - ¹⁶ T. Zhang, Y. Jiang, Z. Song, H. Huang, Y. He, Z. Fang, H. Weng, and C. Fang, *Nature* **566**, 475 (2019).
 - ¹⁷ M. N. Gjerding, A. Taghizadeh, A. Rasmussen, S. Ali, F. Bertoldo, T. Deilmann, N. R. Knøsgaard, M. Kruse, A. H. Larsen, S. Manti, *et al.*, *2D Materials* **8**, 044002 (2021).
 - ¹⁸ N. Mounet, M. Gibertini, P. Schwaller, D. Campi, A. Merkys, A. Marrazzo, T. Sohler, I. E. Castelli, A. Cappelletti, G. Pizzi, *et al.*, *Nature Nanotechnology* **13**, 246 (2018).
 - ¹⁹ D. Campi, N. Mounet, M. Gibertini, G. Pizzi, and N. Marzari, *ACS nano* (2023), 10.1021/acsnano.2c11510.
 - ²⁰ G. Shipunov, B. Piening, C. Wuttke, T. Romanova, A. Sadakov, O. Sobolevskiy, E. Y. Guzovsky, A. Usoltsev, V. Pudalov, D. Efremov, *et al.*, *The Journal of Physical Chemistry Letters* **12**, 6730 (2021).
 - ²¹ P.-J. Guo, X.-Q. Lu, W. Ji, K. Liu, and Z.-Y. Lu, *Physical Review B* **102**, 041109 (2020).
 - ²² C. L. Kane and E. J. Mele, *Physical Review Letters* **95**, 226801 (2005).
 - ²³ B. A. Bernevig and S.-C. Zhang, *Physical Review Letters* **96**, 106802 (2006).
 - ²⁴ M. König, S. Wiedmann, C. Brüne, A. Roth, H. Buhmann, L. W. Molenkamp, X.-L. Qi, and S.-C. Zhang, *Science* **318**, 766 (2007).
 - ²⁵ L. Fu and C. L. Kane, *Physical Review B* **76**, 045302 (2007).
 - ²⁶ G. Giovannetti, P. A. Khomyakov, G. Brocks, P. J. Kelly, and J. Van Den Brink, *Physical Review B* **76**, 073103 (2007).
 - ²⁷ N. D. Drummond, V. Zolyomi, and V. I. Fal'ko, *Physical Review B* **85**, 075423 (2012).
 - ²⁸ D. Grassano, O. Pulci, V. Shubnyi, S. Sharapov, V. Gusynin, A. Kavokin, and A. Varlamov, *Physical Review B* **97**, 205442 (2018).
 - ²⁹ J. L. Collins, A. Tadich, W. Wu, L. C. Gomes, J. N. Rodrigues, C. Liu, J. Hellerstedt, H. Ryu, S. Tang, S.-K. Mo, *et al.*, *Nature* **564**, 390 (2018).
 - ³⁰ C. Zhao, M. Hu, J. Qin, B. Xia, C. Liu, S. Wang, D. Guan, Y. Li, H. Zheng, J. Liu, *et al.*, *Physical Review Letters* **125**, 046801 (2020).
 - ³¹ J. Liu, T. H. Hsieh, P. Wei, W. Duan, J. Moodera, and L. Fu, *Nature Materials* **13**, 178 (2014).
 - ³² X. Qian, J. Liu, L. Fu, and J. Li, *Science* **346**, 1344 (2014).
 - ³³ L. Fu, C. L. Kane, and E. J. Mele, *Physical Review Letters* **98**, 106803 (2007).
 - ³⁴ R.-J. Slager, A. Mesaros, V. Juričić, and J. Zaanen, *Nature Physics* **9**, 98 (2013).
 - ³⁵ J. Kruthoff, J. De Boer, J. Van Wezel, C. L. Kane, and R.-J. Slager, *Physical Review X* **7**, 041069 (2017).
 - ³⁶ H. C. Po, A. Vishwanath, and H. Watanabe, *Nature Communications* **8**, 1 (2017).
 - ³⁷ E. Khalaf, H. C. Po, A. Vishwanath, and H. Watanabe, *Physical Review X* **8**, 031070 (2018).
 - ³⁸ Z. Song, T. Zhang, Z. Fang, and C. Fang, *Nature Communications* **9**, 3530 (2018).
 - ³⁹ D. Campi, N. Mounet, M. Gibertini, G. Pizzi, and N. Marzari, "Materials Cloud two-dimensional crystals database (MC2D)," <https://doi.org/10.24435/materialscloud:36-nd> (2022).
 - ⁴⁰ R. Gillen, S. J. Clark, and J. Robertson, *Physical Review B* **87**, 125116 (2013).
 - ⁴¹ P. Giannozzi, S. Baroni, N. Bonini, M. Calandra, R. Car, C. Cavazzoni, D. Ceresoli, G. L. Chiarotti, M. Cococcioni, I. Dabo, A. D. Corso, S. de Gironcoli, S. Fabris, G. Fratesi, R. Gebauer, U. Gerstmann, C. Gougoussis, A. Kokalj, M. Lazzeri, L. Martin-Samos, N. Marzari, F. Mauri, R. Mazzarello, S. Paolini, A. Pasquarello, L. Paulatto, C. Sbraccia, S. Scandolo, G. Sclauzero, A. P. Seitsonen, A. Smogunov, P. Umari, and R. M. Wentzcovitch, *Journal of Physics: Condensed Matter* **21**, 395502 (2009).

- ⁴² P. Giannozzi, O. Andreussi, T. Brumme, O. Bunau, M. B. Nardelli, M. Calandra, R. Car, C. Cavazzoni, D. Ceresoli, M. Cococcioni, *et al.*, *Journal of Physics: Condensed Matter* **29**, 465901 (2017).
- ⁴³ J. P. Perdew, K. Burke, and M. Ernzerhof, *Physical Review Letters* **77**, 3865 (1996).
- ⁴⁴ D. R. Hamann, *Physical Review B* **88**, 085117 (2013).
- ⁴⁵ M. van Setten, M. Giantomassi, E. Bousquet, M. Verstraete, D. Hamann, X. Gonze, and G.-M. Rignanese, *Computer Physics Communications* **226**, 39 (2018).
- ⁴⁶ D. Gresch, G. Autes, O. V. Yazyev, M. Troyer, D. Vanderbilt, B. A. Bernevig, and A. A. Soluyanov, *Physical Review B* **95**, 075146 (2017).
- ⁴⁷ C. Sgierovello, M. Peressi, and R. Resta, *Physical Review B* **64**, 115202 (2001).
- ⁴⁸ J. Heyd, G. E. Scuseria, and M. Ernzerhof, *The Journal of Chemical Physics* **118**, 8207 (2003).
- ⁴⁹ G. Bergerhoff, I. Brown, and F. Allen, *International Union of Crystallography, Chester* **360**, 77 (1987).
- ⁵⁰ D. Zagorac, H. Müller, S. Ruehl, J. Zagorac, and S. Rehme, *Journal of Applied Crystallography* **52**, 918 (2019).
- ⁵¹ S. Gražulis, A. Daškevič, A. Merkys, D. Chateigner, L. Lutterotti, M. Quiros, N. R. Serebryanaya, P. Moeck, R. T. Downs, and A. Le Bail, *Nucleic Acids Research* **40**, D420 (2012).
- ⁵² P. Villars, M. Berndt, K. Brandenburg, K. Cenzual, J. Daams, F. Hulliger, T. Massalski, H. Okamoto, K. Otsaki, A. Prince, *et al.*, *Journal of Alloys and Compounds* **367**, 293 (2004).
- ⁵³ A. A. Soluyanov and D. Vanderbilt, *Physical Review B* **83**, 235401 (2011).
- ⁵⁴ G. Pizzi, V. Vitale, R. Arita, S. Blügel, F. Freimuth, G. Géranton, M. Gibertini, D. Gresch, C. Johnson, T. Kozetsune, *et al.*, *Journal of Physics: Condensed Matter* **32**, 165902 (2020).
- ⁵⁵ S. Baroni, S. De Gironcoli, A. Dal Corso, and P. Giannozzi, *Reviews of modern Physics* **73**, 515 (2001).
- ⁵⁶ G. Pizzi, A. Cepellotti, R. Sabatini, N. Marzari, and B. Kozinsky, *Computational Materials Science* **111**, 218 (2016).
- ⁵⁷ S. Huber, S. Zoupanos, M. Uhrin, L. Talirz, L. Kahle, R. Häuselmann, D. Gresch, T. Müller, A. V. Yakutovich, C. W. Andersen, *et al.*, arXiv preprint arXiv:2003.12476 (2020).
- ⁵⁸ D. Grassano, D. Campi, A. Marrazzo, and N. Marzari, “2d topological insulators,” <https://www.materialscloud.org/discover/2dtopo> (2022).
- ⁵⁹ Y. Hinuma, G. Pizzi, Y. Kumagai, F. Oba, and I. Tanaka, *Computational Materials Science* **128**, 140 (2017).
- ⁶⁰ See Supplementary Material at [URL] for the atomic structure, band structure, density of states and HWCC evolution (where applicable) of the QSHIs and DGMS identified which include Refs. 12 and 75.
- ⁶¹ G. Gusev, Z. Kvon, E. Olshanetsky, A. Levin, Y. Krupko, J. Portal, N. Mikhailov, and S. Dvoretzky, *Physical Review B* **89**, 125305 (2014).
- ⁶² F. Aryasetiawan and O. Gunnarsson, *Reports on Progress in Physics* **61**, 237 (1998).
- ⁶³ T. V. Menshchikova, M. Otrokov, S. Tsirkin, D. Samorokov, V. Bebeva, A. Ernst, V. Kuznetsov, and E. V. Chulkov, *Nano Letters* **13**, 6064 (2013).
- ⁶⁴ Y. Liu, Y. Li, S. Rajput, D. Gilks, L. Lari, P. Galindo, M. Weinert, V. Lazarov, and L. Li, *Nature Physics* **10**, 294 (2014).
- ⁶⁵ L. Zhou, L. Kou, Y. Sun, C. Felser, F. Hu, G. Shan, S. C. Smith, B. Yan, and T. Frauenheim, *Nano letters* **15**, 7867 (2015).
- ⁶⁶ M. Hirayama, S. Matsuishi, H. Hosono, and S. Murakami, *Physical Review X* **8**, 031067 (2018).
- ⁶⁷ L. Zhou, B. Shao, W. Shi, Y. Sun, C. Felser, B. Yan, and T. Frauenheim, *2D Materials* **3**, 035022 (2016).
- ⁶⁸ Z.-Q. Huang, W.-C. Chen, G. M. Macam, C. P. Crisostomo, S.-M. Huang, R.-B. Chen, M. A. Albao, D.-J. Jang, H. Lin, and F.-C. Chuang, *Nanoscale Research Letters* **13**, 1 (2018).
- ⁶⁹ H. Weng, X. Dai, and Z. Fang, *Physical review X* **4**, 011002 (2014).
- ⁷⁰ N. D. Lowhorn, T. M. Tritt, E. E. Abbott, and J. Kolis, *Applied Physics Letters* **88**, 022101 (2006).
- ⁷¹ A. O’Hare, F. Kusmartsev, and K. Kugel, *Nano Letters* **12**, 1045 (2012).
- ⁷² A. Marrazzo, M. Gibertini, D. Campi, N. Mounet, and N. Marzari, *Physical Review Letters* **120**, 117701 (2018).
- ⁷³ J. Liu, H. Wang, C. Fang, L. Fu, and X. Qian, *Nano Letters* **17**, 467 (2017).
- ⁷⁴ A. Wang, Z. Wang, A. Du, and M. Zhao, *Physical Chemistry Chemical Physics* **18**, 22154 (2016).
- ⁷⁵ K. Momma and F. Izumi, *Journal of Applied Crystallography* **44**, 1272 (2011).

TABLE I: Table containing a collection of direct (DG) and indirect (IG) band gaps (derived from the final calculations on a dense k-point grid), binding energies (E_B) and previous literature references for the QSHIs and DGMs identified. In light gray, those in the previous work by Marrazzo et al.¹² (in absence of strain). For HgNS, both the PBE and HSE gap (in parenthesis) are reported.

	Formula	DG (meV)	IG (meV)	E_B (meV)	Ref.
QSHI	HfBr	233	48	15.8	65,66
	HfTe ₅	299	171	16.5	69
	HgNS	7 (38)	7 (38)	19.4	
	ZrTe ₅	281	220	19.4	69
	Pt ₂ HgSe ₃	178	142	60.2	72
	RhTaTe ₄	67	67	26.4	73
	AsCuLi ₂	65	58	62.7	
	TiCu ₂ Te ₃	6	5	44.0	
	IrNbTe ₄	40	37	27.1	73
	Bi	656	578	17.9	18
	TiNI	20	20	14.6	18,74
	In ₂ ZnS ₄	7	5	36.1	
	TaIrTe ₄	15	15	25.8	73
	DGM	BaCr ₂ N ₂ O ₈	19	-124	11.0
VBr ₃		33	-99	15.1	
FePO ₄ (CH ₃)		11	-58	18.8	
HfCl		264	-166	14.8	65
Fe ₂ O ₃		17	-21	6.4	
MoI ₂ S ₂		47	-117	14.4	
Mo ₂ Ta ₂ O ₁₇		17	-36	10.0	
WTe ₂		738	738	24.7	18,32
MoTe ₂		107	-259	24.5	18,32
ZrBr		45	-19	15.6	11,65
ZrCl		64	-196	14.7	65